PHYSICAL REVIEW D **95,** 044021 (2017)

Classifying self-gravitating radiations

Hyeong-Chan Kim[1,2,*]

[1]*Department of Physics, North Carolina State University, Raleigh, North Carolina 27695-8202, USA*
[2]*School of Liberal Arts and Sciences, Korea National University of Transportation, Chungju 380-702, Korea*

(Received 31 January 2016; revised manuscript received 27 December 2016; published 16 February 2017)

We study a static system of self-gravitating radiations confined in a sphere by using numerical and analytical calculations. Because of the scaling symmetry of radiations, most of the main properties of a solution can be represented as a segment of a solution curve on a plane of two-dimensional scale invariant variables. We define an "approximate horizon" (AH) from the analogy with an apparent horizon. Any solution curve contains a unique point that corresponds to the AH. A given solution is uniquely labeled by three parameters representing the solution curve, the size of the AH, and the sphere size, which are an alternative to the data at the outer boundary. Various geometrical properties including the existence of an AH and the behaviors around the center can be identified from the parameters. We additionally present an analytic solution of the radiations on the verge of forming a black hole. Analytic formulas for the central mass of the naked singularity are given.

DOI: 10.1103/PhysRevD.95.044021

I. INTRODUCTION

A bounded self-gravitating isothermal sphere is an interesting object as a model of a small dense nucleus of stellar systems, which is to some extent independent of the outer parts of the system [1]. In 1981, a spherically symmetric solution of self-gravitating radiation was presented by Sorkin *et al.* [2] as a solution that maximizes the entropy based on general relativity. The heat capacity and stability of the solution were further analyzed in Refs. [3] and [4–6]. Schmidt and Homann [7] named the geometry "photon star." Thereafter, the system has drawn attention repeatedly in relation to the entropy bound [8,9], maximum entropy principle [10–12], holograpic principle [13–15], black hole thermodynamics [16], and exclusion of black hole firewalls [17]. Self-gravitating radiation in anti–de Sitter spacetime was also pursued [18–20]. Studies on the systems of self-gravitating perfect fluids are undergone [21]. An interesting extension of the self-gravitating system was presented in Ref. [7,22] where a conical singularity is included at the center as an independent source from the radiation. The singularity was said to be benign in the sense that it does not give rise to inextensible causal geodesics, because no timelike geodesics reach the singularity and null geodesics simply pass it. A thermodynamic interpretation for the conical singularity was also discussed [22]. Analytic analysis was presented for an extreme case, which was interpreted as a spacetime black hole with perfect fluid in equilibrium [23]. Some of the singular solutions were shown to have an interesting geometry, which resembles an event horizon to an outside observer. The similarity was used to understand the near horizon geometry of a black hole [24].

Let the sphere of radiation have a radius R. Outside the sphere, the spacetime is described by the vacuum Schwarzschild metric with Arnowitt-Deser-Misner (ADM) mass M_R. The system is different from an ordinary star whose boundary is implemented by its own gravity and equation of state. In the absence of an artificial boundary at R, the density of the static solution becomes proportional to $1/r^2$ as $r \to \infty$. Then, the energy of the system goes to infinity and stability issues arise. Despite this difference, we call it a star later in this work for convenience. The metric inside was shown [22] to be given by

$$ds^2 = -\left(1 - \frac{2M_R}{R}\right)\sqrt{\frac{\rho(R)}{\rho(r)}}dt^2 + \frac{dr^2}{1 - 2m(r)/r} + r^2(d\theta^2 + \sin^2\theta d\phi^2), \qquad r \le R, \tag{1}$$

where $m(r)$ and $\rho(r)$ are the mass inside and the density at r, respectively. The energy density is related with the mass as

$$\rho(r) = \frac{1}{4\pi r^2}\frac{dm(r)}{dr}. \tag{2}$$

Because the star is composed of radiations, it also satisfies $\rho(r) = 3p(r)$, where $p(r)$ denotes the pressure at r. From the black body radiation law, the surface energy density is given by $\rho(R) = \sigma T^4$, where $T \equiv (1 - 2M_R/R)^{-1/2}\beta^{-1}$ denotes the locally measured temperature at R and σ is the Stefan-Boltzmann constant. In summary, a solution of the spherically symmetric self-gravitating radiation can be uniquely specified by using the boundary data,

*hckim@ut.ac.kr

$$\mathfrak{B} \equiv (R, M_R, T). \tag{3}$$

The structure of the star is described by the Tollman-Oppenheimer-Volkoff (TOV) equation for the metric (1). Introducing a dimensionless variable

$$u \equiv \frac{2m(r)}{r}, \tag{4}$$

the TOV equation can be cast into a second order differential equation for u as

$$\frac{1}{6}(u+u')(u+u'+3) + (u-1)\left(u+u'-\frac{u'+u''}{4}\right) = 0, \tag{5}$$

where prime denotes the derivative with respect to a dimensionless variable

$$\xi = \log\frac{r}{r_H}, \tag{6}$$

and r_H is a length scale that is specified later. Equation (5) does not contain any length scale. Therefore, the system possesses a scaling symmetry: The transformation $(m \to e^s m, r \to e^s r)$ preserves the equation of motion. As a result, various properties of the solutions can be described by scale-invariant variables. Introducing a scale-invariant variable v,

$$v \equiv \frac{dm(r)}{dr} = 4\pi r^2 \rho(r) = \frac{u+u'}{2}, \tag{7}$$

the TOV equation (5) can be rewritten as a first order differential equation for u and v,

$$\frac{dv}{du} = f(u,v) \equiv \frac{2v(1-2u-2v/3)}{(1-u)(2v-u)}. \tag{8}$$

The integral curve of Eq. (8) on the (u, v) plane is called a solution curve, which is denoted by C in this work. The allowed range of (u, v) is $u < 1$ and $v \geq 0$, where each inequality represents the fact that the spacetime is static and the energy density of radiation is non-negative, respectively. For this reasons, we call $u = 1$ and $v = 0$ the static boundary (SB) and the positive energy boundary (PB), respectively. From Eq. (8), one may easily notice that any solution curve becomes parallel to the u axis when it crosses the PB and the line

$$P: 2u + 2v/3 = 1 \tag{9}$$

and parallel to the v axis when it crosses the SB and the line

$$H: u = 2v. \tag{10}$$

Therefore, the solution curve cannot cross the two boundaries, the SB and PB. This property also indicates that a solution curve spirals around the point $(u, v) = (3/7, 3/14)$, which is an end of every solution curve. The solution curves are divided into two classes by means of the other end, which corresponds to the center of the star. One class is composed of a solution curve beginning at $(u, v) = (0, 0)$. The solution curve, namely C, describing solutions of pure radiations was found in Ref. [2] as a stable static configuration, where the word pure implies that the star does not contain mass contributions other than the radiation. The other class of solution curves describes spacetimes bearing a negative mass source at the center that presents a conical singularity. The curves originate from $(u, v) \to (-\infty, 0)$.

However, we notice that the understanding on the details of the geometry is still incomplete because its geometric structure is not classified systematically and analyzed thoroughly. The purpose of the present work is to make up for this part. For the manuscript be self-consistent, we have taken some of the previous results from the literature, which are in Secs. II A, II B, II C, III A, and part of Sec. IV. One of the main purposes of this work is to characterize the spherically symmetric star of self-gravitating radiations by means of parameters representing their physical characteristics. A solution corresponding to the second class was known to have a wall (deformed horizonlike object) that was named the approximate horizon (AH) in Ref. [24]. As a first step to accomplish this purpose, in Sec. II D, we present a clear definition for the AH from the analogy with an apparent horizon. Following the definition, each solution curve has a point corresponding to the AH irrespective of the existence of central singularity. As a second step, in Sec. II E, we classify the solution curves in terms of a physical parameter ν defined at the AH, where the value of ν is given by the distance of the solution curve C_ν from the SB. Because the set of all possible solution curves sweeps every physically acceptable point in the (u, v) plane, any point on the plane can equivalently be named by using ν and a parameter ξ representing the position on the curve. Now, a solution of self-gravitating radiation is uniquely determined by the scale of the system, which is fixed by the radius of the AH, r_H. A solution is uniquely described by using the boundary data in Eq. (3). Even though intuitive for an outside observer, this is inconvenient to describe the internal structure of the self-gravitating radiations contrary to the description by using $(\nu, r_H, R \equiv r_H e^\xi)$.

We also present the general behaviors of solution curves including the singular one in Sec. III B. Solution curves for various ν are presented and their behaviors are explained. Specifically, the behaviors of solutions are given as functions of ν around various positions including the center, the maximal v position, and the AH. This compliments the shortage of the numerical calculation to find a solution curve. In Sec. IV, we provide an analytic solution

describing the star on the verge of forming a black hole composed of self-gravitating radiations. This is a generalization of the analytic analysis done in Refs. [23,24]. We summarize and discuss the results in Sec. V.

II. PROPERTIES FOR SELF-GRAVITATING RADIATION

A. Scale transformation

Let us parametrize a solution curve C_ν of Eq. (8) in terms of ξ as $(u(\xi), v(\xi))$, where ν is a parameter characterizing the curve that is specified in Sec. II E. The parametrization is determined by Eq. (7), which presents the radius, $r(\xi)$. Note that, from Eq. (6), the values of u and v at each point on the curve are invariant under the scaling,

$$\begin{aligned} &m \to \overline{m} = e^s m, \qquad r \to \overline{r} = e^s r, \\ &\xi \to \overline{\xi} = \xi + s, \qquad u(\xi) \to \overline{u}(\overline{\xi}) = u(\xi), \\ &v(\xi) \to \overline{v}(\overline{\xi}) = v(\xi). \end{aligned} \tag{11}$$

Therefore, $\overline{u}(\xi) = u(\xi - s)$ represents a new solution of Eq. (5) with its mass, density, and radius scaled. Explicitly, the surface values (u_R, v_R) are invariant,

$$\begin{aligned} \overline{u}(\xi_R + s) &= u(\xi_R) = \frac{2M_R}{R}, \\ \overline{v}(\xi_R + s) &= v(\xi_R) = 4\pi R^2 \rho(R), \end{aligned} \tag{12}$$

where $M_R = m(R)$. On the other hand, the mass, the radius, and the density scale as

$$\overline{m}(e^s R) = e^s M_R, \qquad \overline{R} = e^s R, \qquad \overline{\rho}(e^s R) = e^{-2s}\rho(R). \tag{13}$$

In addition, the range of ξ is changed from $(-\infty, \xi_R]$ to $(-\infty, \xi_R + s]$. Given a solution $u(\xi)$ supported with the boundary value at $r = R$, the scale transformation provides a set of solutions having scaled mass and density related by Eq. (13). In fact, any point on C_ν can play the role of a boundary point that supports a set of solutions related by the scale transform. In this sense, a solution curve C_ν provides a set of solutions parametrized by R and s.

B. The central region

Let us study the behaviors of the solutions to Eq. (5) around the origin with $\xi \ll -1$. Equation (5) allows two different small r behaviors,

$$m_{\rm r}(r) = \frac{\kappa r_H}{6}\left(\frac{r}{r_H}\right)^3, \qquad m_{\rm s}(r) = \frac{r_H}{2}\left[-\mu_0 + \frac{\kappa}{5}\left(\frac{r}{r_H}\right)^5\right]. \tag{14}$$

We scale the mass and radius in terms of r_H to encompass the scale symmetry. The first one, $m_{\rm r}(r)$, corresponds to the regular solution that is discussed in Sec. III A. The second one, $m_{\rm s}$, must be negative at the origin, implying $\mu_0 > 0$. Because the radiation has positive energy density, κ is required to be positive. The energy density of radiation at the center is $\rho_{\rm s} = (\kappa/8\pi r_H^2) \times (r/r_H)^2$. Comparing the functional forms of $\rho_{\rm s}$ with $\rho_{\rm r}$, it is evident that the radiation is repelled from the center by the negative mass at the central singularity.

We next consider how the solutions (14) change with respect to the scaling. Through the scale transformation (11), the coefficients κ and μ_0 should change. Let us consider the case of regular solution, $m_{\rm r}(r)$, first. Under the scaling in Eq. (11), the functional form of $m_{\rm r}$ in Eq. (14) changes to

$$\overline{m}_{\rm r}(\overline{r}) = e^s m_{\rm r}(r) \Rightarrow \overline{m}_{\rm r}(\overline{r}) = \frac{\kappa \overline{r}_H}{6}\left(\frac{\overline{r}}{\overline{r}_H}\right)^3, \tag{15}$$

where we use the transformation law of the referential point (13) and $\overline{r}_H = e^s r_H$ is the transformed radius of r_H. Omitting bar in $\overline{r}$ in Eq. (15), the functional form of the scaled solution is the same as the original one with the replacement $\kappa \to \kappa e^{-2s}$. Therefore, once one finds a solution for given κ, the central form of all other solutions related by the scaling is also at hand.

For the case of the solution $m_{\rm s}(r)$, the scaling (11) leads to

$$\overline{m}_{\rm s}(\overline{r}) = \frac{\overline{r}_H}{2}\left[-\mu_0 + \frac{\kappa}{5}\left(\frac{\overline{r}}{\overline{r}_H}\right)^5\right]. \tag{16}$$

Note that the functional form of the scaled solution is, omitting the bar in $\overline{r}$, the same as the original one with the replacements $\mu_0 \to e^s \mu_0$ and $\kappa \to e^{-4s}\kappa$. With this form, the explicit functional dependence on the scale becomes evident. Note that the mass, $-\overline{r}_H \mu_0$, of the conical singularity changes with the scale.

C. Asymptotic behaviors

We next consider the asymptotic behavior as $\xi \to \infty$. By assuming solutions in the form, $u = ae^{-\xi} + b$, one may find that the differential equation (5) allows two different asymptotic forms for $u(\xi)$,

$$u_a \to \frac{3}{7}, \qquad u_t \to ae^{-\xi}, \tag{17}$$

where a is an arbitrary constant. With the increase of ξ, u_a acts as if it is an attractor that pulls every nearby solution (here, we interpret ξ as if it is a time even though it is a radial coordinate). Introducing a small perturbation, the solution of Eq. (5) with first nonvanishing contribution takes the form

$$u_a = \frac{3}{7}\left[1+\tilde{c}_1 e^{-3\xi/4}\cos\left(\frac{\sqrt{47}}{4}\xi+\tilde{\phi}\right)\right] \Rightarrow m_a(r)$$
$$= \frac{3r}{14}\left[1+\tilde{c}_1\left(\frac{r_H}{r}\right)^{3/4}\cos\left(\frac{\sqrt{47}}{4}\log\frac{r}{r_H}+\tilde{\phi}\right)\right], \quad (18)$$

where $\tilde{c}_1$ and $\tilde{\phi}$ are integration constants. On the (u,v) plane, the curves satisfy

$$\left(u-\frac{3}{7}\right)^2+\frac{64}{47}\left(v-\frac{3}{8}u-\frac{3}{56}\right)^2=\left(\frac{3\tilde{c}_1}{7}\right)^2\left(\frac{r_H}{r}\right)^{3/2}. \quad (19)$$

The solution curves spire in to the point $(u,v)=(3/7,3/14)$ as r increases. For the asymptotic form (18), the scale transform (11) is achieved by $r_H \to \overline{r}_H$.

The other asymptotic form, $u_t(\xi)$, approaches 0 and $v_t(\xi)=0$ for all ξ. The asymptotic form plays the role of an attractor when the radius r (equivalently ξ) decreases from infinity. Small perturbations around u_t,

$$u = u_t+\delta(\xi) = ae^{-\xi}+\epsilon e^{2\xi} \Rightarrow m_t(r) = \frac{a}{2}+\frac{\epsilon}{2}\left(\frac{r}{r_H}\right)^3, \quad (20)$$

increase indefinitely as $r\to\infty$ and the solution leaves u_t permanently, where ϵ is a tiny integration constant. However, as is shown later, in the presence of an AH close to an apparent horizon, this almost constant mass region becomes wide enough to regard Eq. (20) as an approximate asymptotic form for $r \gg r_H$.

Equation (17) may not be realized unless the outer boundary is located in the asymptotic region. For most cases, noting the heat capacity in Ref. [3], an instability appears at a smaller radius than r_H, which makes the star unstable. However, as noted in Ref. [22], the conical singularity may play some role in thermodynamics and affects the stability. In this sense, the issue of stability needs additional research.

D. Approximate horizon

Solutions other than the regular one have a conical singularity at the center [22]. Based on Newtonian gravity, objects having positive masses attract each other. Similarly, the radiations are attracted to the center due to their self-gravity. On the other hand, the negative mass at the center repels the radiations. The balance of the two behaviors concentrates the radiations at some intermediate region. Therefore, in the presence of large negative mass at the center and a large quantity of radiations outside, enough to compensate the repulsion, a region of strong gravity develops. To represent this phenomenon, we define an AH.

Consider a metric of the form

$$ds^2 = h_{ab}(x^c)dx^a dx^b + r^2 d\Omega_{(2)},$$

where a, b, $c=0$, 1 and $r(x^a)$ is a scalar function of x^0 and x^1. An apparent horizon for the metric is defined by the surface satisfying

$$\chi^2 \equiv h^{ab}\nabla_a r \nabla_b r = 0. \quad (21)$$

At the apparent horizon, the vector field $\nabla_a r$ becomes null. For the metric ansatz (1), the coordinate change $dr\to 0$ for a finite proper distance change $\delta r = \sqrt{g_{rr}}dr$. Applying Eq. (21) to the metric (1), the apparent horizon exists only at the position satisfying $\chi^2 = 1-2m(r)/r = 0$. Equation (8) indicates that this condition is never achieved with the self-gravitating radiation because $du=0$ at the SB, which implies that a solution curve never crosses the SB.

If χ^2 is very small at a surface surrounded by thermal radiations, an observer located outside of the region has difficulty distinguishing the surface from an apparent horizon. Even though photons may propagate over the surface, it would be difficult to discern it from the surroundings. In this sense, we define an AH as a surface where χ^2 takes its minimum value for a given solution curve. The local minimization condition of χ^2 for the metric (1) becomes

$$\delta(\chi^2)=0 \Rightarrow u=2v, \qquad \frac{3}{7}<u\le 1, \quad (22)$$

where the inequality is included because χ^2 is locally maximized on H for $u<3/7$. Noting the asymptotic form (19), a solution curve crosses the line H many times. Of all the points, the nearest one to the SB corresponds to the AH. In fact, as can be seen in the next section, every AH is located in the region $u_r \le u < 1$, where $u_r \approx 0.4926$ corresponds to the AH value of the regular solution.

E. Characterizing solution curves

In Refs. [2,4,22], the authors identified the solution space in terms of a set of parameters defined at the surface $r=R$. To do this, Eq. (5) was integrated to obtain the solution curve C inward to $r=0$ after fixing the boundary value (u_R, v_R). A lesson from the experiences on the regular solution is that a solution space is conveniently characterized by the combination of a point (u_R, v_R) on the solution curve and the radius R of the system as in Fig. 1. The whole solution space can be found once one finds a set of solution curves covering a whole physically acceptable region of the (u,v) plane. Because the (u,v) plane is two dimensional, the one-dimensional solution curves should be characterized by one parameter, namely, ν. An immediate task is to find out the most convenient parameter for ν. A first impression is to use the central values such as μ_0 or κ in Eq. (14). For example, with the choice of a scaling $e^s=\kappa^{1/4}$, one can choose $\nu \equiv \overline{\mu}_0 = \mu_0\kappa^{1/4}$ with $\overline{\kappa}=1$. This choice is relevant theoretically only for singular

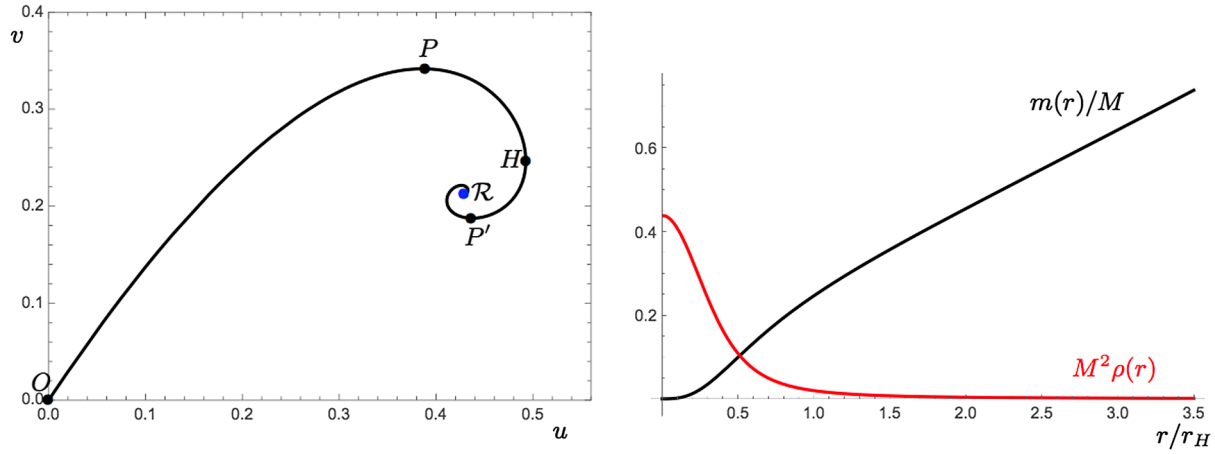

FIG. 1. The solution curve and typical form for the mass and density profile for a regular solution. The solution curve in the left panel reproduces Fig. 1 in Ref. [22]. Each point on C corresponds to a boundary data for a regular solution.

solutions and the behaviors of the solution are too sensitive to a small change of the central values numerically.

In the present work, we choose to characterize the solution curve in terms of the distance of the solution curve to the SB,

$$\nu \equiv 1 - u_H. \tag{23}$$

Because any solution curve spires in to the point $\mathcal{R}$, it meets the line H indefinite number of times. To avoid multiple labeling, we should restrict the value of ν so that any solution curve has only one name. This can be achieved by restricting the value of ν so that its maximum value corresponds to that of the regular solution $\nu_r \approx 0.50735$, the value of which can be determined from the results in Ref. [2]. Now, the line H is given by

$$H \equiv \left\{ H_\nu \left(1-\nu, \frac{1-\nu}{2} \right) | 0 < \nu \le \nu_r \right\}, \tag{24}$$

where the absence of horizon restricts $\nu > 0$.

For a given C_ν, the value of u is maximized to be $u_H = 1-\nu$ at H_ν. By using the scale transform, we may freely choose a referential solution so that $\xi = 0$ at H. Let us consider a system given by the boundary data (R, M_R, T_R). The boundary values for the scale-invariant variables are given by $u_R = 2M_R/R$ and $v_R = 4\pi\sigma R^2 T_R^4$. The solution curve can be parametrized by $\xi = \log(r/r_H)$. Then, the position of the boundary data (u_R, v_R) on the solution curve can be uniquely represented once $\xi_R = \log(R/r_H)$ is known. Therefore, a specific solution is uniquely determined once we know

$$(\nu, r_H, R). \tag{25}$$

Now, it is easy to identify whether or not there is an AH. If ξ_R is positive, the star size R is larger than r_H and a AH exists. Under the scale transformation, (ν, r_H, R) is mapped to $(\nu, e^s r_H, e^s R)$. ξ_R is invariant because it is defined from the ratio of two radius of the star and of the AH; both are covariant.

III. VARIOUS SOLUTIONS

Any point (u_R, v_R) on the solution curve C_ν can play the role of boundary data at $r = R$. Because of the scale invariance (12), a given point (u_R, v_R) represents a one parameter family of boundary data, $\{(e^s M_R, e^s R, e^{-2s} T), s \in \Re\}$, characterized by the scaling s. Rather than using the boundary data, we characterize a solution by identifying (ν, r_H, R).

A. Regular solutions

Before dealing general solutions, let us illustrate a well-known solution in Refs. [2–4]. Most results in this subsection are reproductions of these works except for a few details. The purpose of this subsection is to illustrate the role of a solution curve C in the (u, v) plane obtained by numerical integration of Eq. (8) or Eq. (5). The curve C is given in the left panel of Fig. 1. An important property of the solution curve is its uniqueness. The value ν_r presented just after Eq. (24) is given by obtaining $u_H \approx 0.4926$ for the solution curve. A typical mass and density profiles for a specific solution are shown in Fig. 1(b).

The solution curve C begins with $u = 0 = v$ at $r = 0$. On the curve v takes its maximal value $v_P \approx 0.3416$ at P and u takes its maximum u_H at H. The ratio of the radial coordinates between P and H is $r_P/r_H \equiv e^{\xi_P} \approx 0.4823$. The allowed range of u and v is restricted to $0 \le u \le u_H$ and $0 \le v \le v_P$, respectively. Eventually, the curve spires in to the point $\mathcal{R}(3/7, 3/14)$. From the analysis of the heat capacity in Ref. [3], a thermodynamic instability is set for a system having the outer boundary in the region from P to H. Interestingly, the heat capacity for a system having the outer boundary just outside the point H is positive definite.

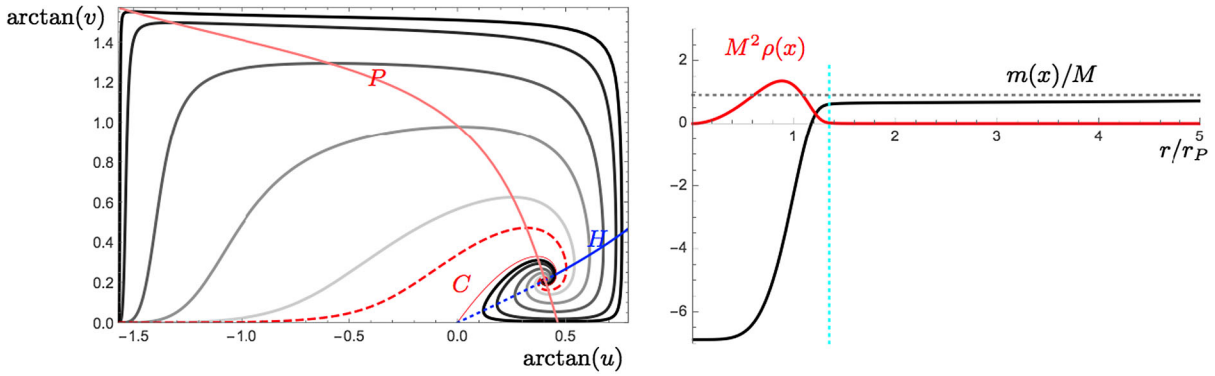

FIG. 2. The solution curves (left), mass, and density distribution (right). In the left panel, each curve corresponds to $\nu = \nu_r$, 0.45, 0.4, 0.3, 0.2, 0.1, and 0.05, respectively from the bottom. The blue curve H represents the referential position given in Eq. (10). The thick pink curve P denotes the position where v is maximized on solution curves in Eq. (9). In the right panel, the typical behavior of mass and density is given. This figure corresponds to $\nu = .1$. The dotted cyan line denotes where a AH forms.

The density at the center is $\rho(0) = \kappa(8\pi r_H^2)^{-1}$, where $\kappa \approx 4.759$, and monotonically decreases with r. The central form of mass is given by $m_{\rm r}(r)$ in Eq. (14). For $r \gg r_H$, the mass increases linearly.

B. Solutions with a conical singularity at the center

In the left panel of Fig. 2, we plot solution curves for several different values of ν to show their characteristic behaviors. In the right panel, the typical behaviors of the mass and the density for $\nu < \nu_r$ with respect to the radius are additionally displayed. As in Eq. (23), ν represents the closest distance from the SB to the solution curve C_ν. Therefore, along H, a solution curve with a smaller ν is nearer to the SB than that with a larger one. The solution curve $C \equiv C_{\nu_r}$ representing the regular solution is the farthest one from the SB in weak red form. A solution curve C_ν with $0 < \nu < \nu_r$ is located outside of it and the corresponding solution has a conical singularity at the center. The radius r increases as one tracks a given solution curve C_ν in $\mathcal{R}$ in Fig. 1. This result comes from Eq. (7), which gives $d\xi = du/(2v - u)$. From this one notices that the radius of the sphere in Eq. (6) grows when u increases above H and decreases below H. Because the gradient of u changes sign on H, the radius monotonically increases if one traces the solution curve inward. In addition, the solution curve spirals in to the point $\mathcal{R}$ as $r \to \infty$ because it should be horizontal (vertical) on P (H) and should not cross itself.

Differences of C_ν from the regular-solution curve C are apparent for small r. The curves begin at $(u, v) \to (-\infty, 0)$ at $r = 0$, where the negative value of u is due to the negative mass of conical singularity, $m(0) = -\mu_0 r_H/2$. In addition, the density of the radiations vanishes at the center and increases quadratically with r. Comparing the result of the regular solution where the density takes maximum value at the center, the repulsive nature of the central negative mass to positive energy radiation is apparent. From Eqs. (4), (7), and (16), one may find that $vu^4 \approx \kappa\mu_0^4/2$ for $r \sim 0$. Therefore, a solution curve C_ν stays close to the PB for $u \ll 0$. The size of $\kappa\mu_0^4/2$ determines how fast the solution curve departs the PB. An interesting observation is that both κ and μ_0 are not independent variables but are functions determined by the value of ν only, the functions of which are numerically plotted in Fig. 3. Both monotonically decrease with ν and diverge inverse quadratically as $\nu \to 0$. Numerically, the graphs in Fig. 3 are well approximated by

$$\begin{aligned}\mu_0 &\approx 0.0771\nu^{-2} + 0.2136\nu^{-1} - 1.2077 + 1.0067\nu + \ldots,\\ \kappa &\approx 1.049\nu^{-2} + 5.872\nu^{-1} + 12.93 + 71.90\nu\\ &\quad - 114.7\nu^2 + \ldots,\end{aligned} \tag{26}$$

where the range is $0 < \nu < \nu_r$. A discrepancy of this numerical result is that the plots in Fig. 3 fail to reproduce the regular solution result for $\nu = \nu_r$ where $\mu_0 = 0$ and $\kappa \approx 4.759$. This is because the equations in Eq. (26) are expanded around $\nu = 0$. Let us consider the case with $\nu \sim 0$ briefly. Because $\kappa\mu_0^4 \propto \nu^{-10} \gg 1$, the value v of a solution curve can be nontrivially large even for large negative u. The size of v is comparable to that of $|u|$ when they are of $O(\nu^{-2})$.

As the radius increases, the value of v is maximized at the point P_ν where C_ν crosses P. The maximum value of $v = v_{P_\nu}$ monotonically increases as ν decreases from ν_r. The value of $u_{P_\nu} = 1/2 - v_{P_\nu}/3$ at the maximum point is plotted in the right panel of Fig. 4. The graph can be approximated to be

$$\begin{aligned}u_{P_\nu} &\approx -0.03558\nu^{-2} - 0.1271\nu^{-1} + 0.9246\\ &\quad - 0.3858\nu + \ldots.\end{aligned}$$

For $\nu \ll 1$, it behaves inverse quadratically as expected in the previous paragraph. The value r_{P_ν}/r_H decreases with ν

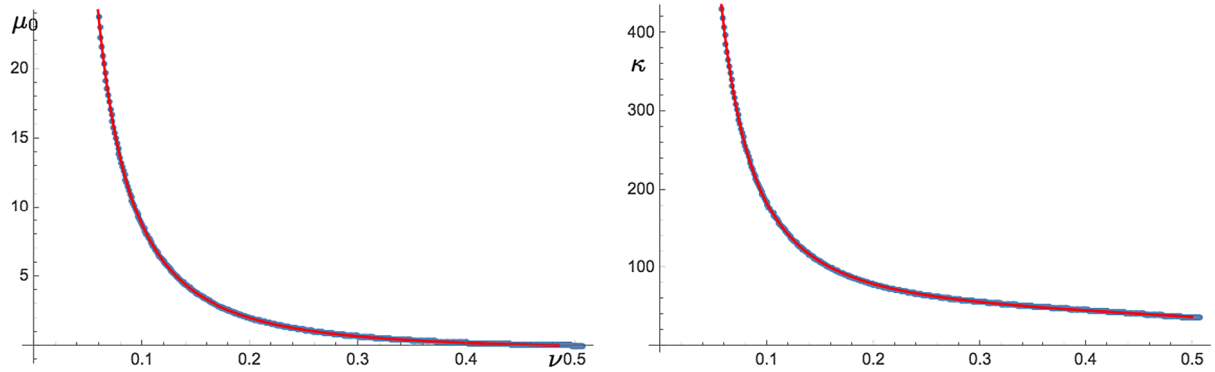

(a) μ_0 as a function of ν. (b) κ as a function of ν.

FIG. 3. The change of μ_0 and κ as a function of ν. The approximate functional forms are given as red curves.

as in the left panel of Fig. 4. The function can be approximated to be

$$\frac{r_P}{r_H} = 0.7807 - 0.4519\nu - 0.3383\nu^2 + \ldots. \tag{27}$$

At $\nu = \nu_r$, the ratio becomes $r_P/r_H \approx 0.4823$, the value of which is the same as that of the regular solution. Note that the ratio and u_{P_ν} are functions of ν only, i.e., they are independent of the boundary choice and the scale. For $u > u_P$, the value of v decreases until the solution curve meets the line P once more.

As the radius further increases, the value of u is maximized at the point H_ν where C_ν crosses the line H. The maximum value of u and the corresponding value for v is given by

$$u_H = 1 - \nu, \qquad v_H = \frac{1-\nu}{2}. \tag{28}$$

Around the point H_ν, the small ν behavior of C_ν is interesting. The density gradient becomes large because $dv/d\xi \propto (1-u)^{-1} \approx \nu^{-1}$. On the other hand, the mass gradient may not be large because $du/d\xi = du/dv \cdot dv/d\xi$ is $O(1)$. A detailed analysis for the behavior of the solution curve is displayed in the next section.

When the solution curve is located below the line H, the value of u starts to decrease with r until C_ν meets H again. Outside the point, C_ν converges gradually to that of the regular solution as it spires in to the point $\mathcal{R}$ in Fig. 1. The asymptotic approach is described by Eq. (19).

IV. ANALYTIC TREATMENT OF A SELF-GRAVITATING RADIATION ON THE VERGE OF FORMING A BLACK HOLE

The geometry around an AH with $\nu \sim 0$ is an especially interesting object because it is on the verge of becoming a true event horizon in the sense that $m(r_{\rm fh}) \approx r_{\rm fh}/2$. We hope that this interesting case allows an analytic description, which turns out to be true. Part of the present results were given in Refs. [23,24]. In Ref. [23], the authors assumed the temperature to be the Hawking temperature. In the present work, we do not take the assumption because it is not always proper. An AH is different from a black hole horizon even though it has some similarity. In Ref. [24], the author analyzed the near AH geometry analytically. Equations (29) and (32) overlap with Eqs. (71) and (66) in

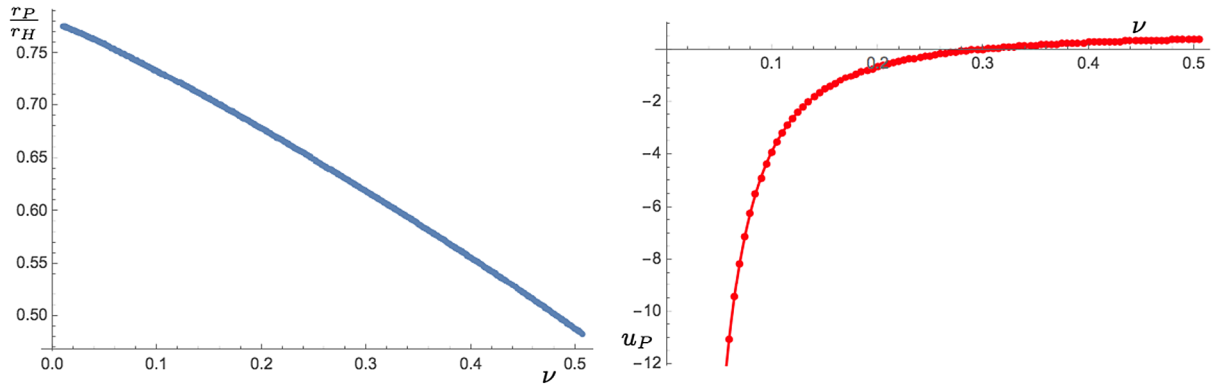

FIG. 4. The values of r_P/r_H and u_P with respect to ν.

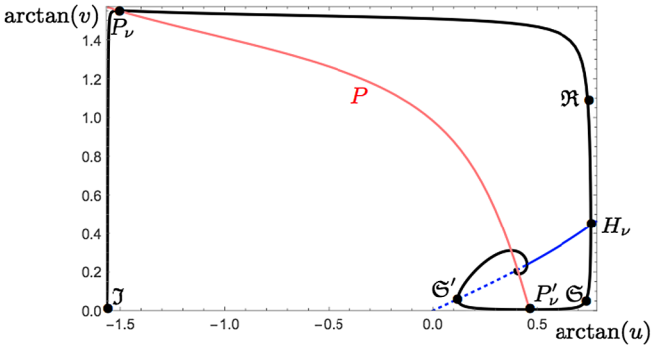

FIG. 5. Solution curve (black) for systems having strong AH. The point $\mathfrak{I}$ represents $(u, v) = (-\infty, 0)$.

Ref. [24], respectively. We extend their analysis to include the whole range of the system.

A solution curve C_ν is given in Fig. 5. For simplicity, we represent a segment of the solution curve by using its boundary points. For example, $[P_\nu, \mathfrak{R}]$ represents the segment from the point P_ν to the point $\mathfrak{R}$. An AH is in the segment $[\mathfrak{R}, \mathfrak{S}]$. There, u is almost constant but v changes a lot. The segment $[\mathfrak{S}, \mathfrak{S}']$ is located just outside of the AH. v remains close to 0 and u decreases monotonically with r. For $\nu \approx 0$, most of the mass is located inside the AH.

First, let us analyze the segment $[\mathfrak{R}, \mathfrak{S}]$ of the solution curve depicted in Fig. 5, which denotes the region near the AH. On the segment, u changes slowly with $u \approx u_H \approx 1$. Solving Eq. (8) keeping first nonvanishing corrections of $O(\nu)$, one gets

$$1 - u \approx \varepsilon \frac{(2v/3 + 1)^2}{\sqrt{2v}} + O(\varepsilon^2),$$
$$\frac{1}{2}\varepsilon^2 \ll v_{\mathfrak{S}} < v < v_{\mathfrak{R}} \ll \frac{1}{2}\left(\frac{9}{\varepsilon}\right)^{2/3}, \tag{29}$$

where $\varepsilon = 9\nu/16$ is the expansion parameter. We choose the points $\mathfrak{R}$ and $\mathfrak{S}$ so that $v_{\mathfrak{R}} = \varepsilon^{-1/3}$ and $v_{\mathfrak{S}} = \varepsilon^{2/3}/2$. Integrating Eq. (7) and using Eq. (6), we get

$$r = r_H e^{\xi}; \qquad \xi = \frac{\varepsilon}{\sqrt{2v}}\left(1 - \frac{v}{6}\right) - \frac{11\varepsilon}{12}, \tag{30}$$

where we choose $\xi = 0$ at H $(v = 1/2)$. Note that r changes only a bit for a large change of v in $[\mathfrak{R}, \mathfrak{S}]$. The mass inside r is, keeping to the dominant corrections, given by

$$m(r(v)) = \frac{r_H}{2} e^{\xi} u \approx \frac{r_H}{2}\left[1 - \frac{\varepsilon(2v)^{3/2}}{9}\left(1 + \frac{27}{8v}\right) - \frac{11\varepsilon}{12}\right]. \tag{31}$$

The relative increase of the mass from $\mathfrak{R}$ to $\mathfrak{S}$ is $(m_{\mathfrak{S}} - m_{\mathfrak{R}})/m_{\mathfrak{R}} \approx 2^{3/2}/9 \times \varepsilon^{1/2}$, which is relatively small compared to $m_{\mathfrak{R}}$. On the other hand, the density, $\rho = v/4\pi r^2$, decreases rapidly in $[\mathfrak{R}, \mathfrak{S}]$ so that $\rho(r_{\mathfrak{S}})/\rho(r_{\mathfrak{R}}) \approx \varepsilon/2$, because ρ is roughly proportional to v. This implies that the density profile in r is extremely steep.

We next analyze the segment $[\mathfrak{S}, \mathfrak{S}']$ of the solution curve depicted in Fig. 5, where $u_{\mathfrak{S}} \approx 1$ and $0 < u_{\mathfrak{S}'} \ll 1$. In the region of interest, $v \ll 1$ and $dv < du$. The solution curve C_ν, solving Eq. (8) up to first nonvanishing order, is described by

$$v = \frac{\varepsilon^2}{2u^2(1-u)^2};$$
$$\varepsilon^{2/3} \ll u_{\mathfrak{S}'} \equiv \varepsilon^\beta < u < u_{\mathfrak{S}} = 1 - \varepsilon^{2/3}. \tag{32}$$

We identify the two curves in Eqs. (29) and (32) at $\mathfrak{S}$, satisfying $du = dv$. The radius can be obtained by integrating Eq. (7) using Eq. (32). To the first nonvanishing correction, we get

$$r = r_H e^{\xi} \approx \frac{r_H}{u}\exp\left[-\frac{11\varepsilon}{12} + \frac{\varepsilon^2}{3u^3}\right] \Rightarrow$$
$$u \approx \frac{r_H}{r}\left[1 - \frac{11\varepsilon}{12} + \frac{\varepsilon^2}{3}\left(\frac{r}{r_H}\right)^3\right], \tag{33}$$

where we keep terms to $O(\varepsilon^1)$ and we choose $\beta = 1/3$. Now, the range of the radius for the segment is given by $r_H < r < \varepsilon^{-1/3} r_H$. The radius increases almost inverse linearly with u. The segment $[\mathfrak{S}, \mathfrak{S}']$ corresponds to the long quasiasymptotic region given by $u_t(\xi)$ in Eq. (20). Note that the mass $m(r) = r_H/2$ is included in the surface $r = (11/4\varepsilon)^{1/3} r_H$.

Outside the surface $\mathfrak{S}'$, near $0 < u$, $v \ll 1$, the solution curve approaches that of the regular solution. The function u takes exactly the same form as that in Eq. (33). On the other hand $v = (\varepsilon^2/2) \times (r/r_H)^2$. Therefore, from the point of view of a far outside observer, the geometry appears to be a combination of a constant point mass, $M = r_H(1 - 11\varepsilon/12)/2$, surrounded by a constant density, $\rho_0 = \varepsilon^2/(8\pi r_H^2)$. This result determines a local temperature uniquely,

$$T = \frac{1}{(8\pi\sigma)^{1/4}}\sqrt{\frac{\varepsilon}{r_H}}.$$

We next consider the segment $[\mathfrak{I}, \mathfrak{R}]$ that corresponds to the region far inside the AH. In the region, $1 - u \gg 0$ and $2v + 1 - u \gg 1$. As was done in Ref. [23], Eqs. (8) and (7) can be approximately solved to give

$$v \equiv \frac{15/2}{(r_H/r)^5 - 1}(1 - u) = \frac{1}{2}\left(\frac{3}{5\varepsilon}\right)^2\left(\frac{r}{r_H}\right)^4\left[1 - \left(\frac{r}{r_H}\right)^5\right]^2. \tag{34}$$

v takes its maximum value $v_{\max} = (7/2)^{1/5} 9/7^3 \epsilon^2$ at $r = r_{\max} \equiv (2/7)^{1/5} r_H$, where the integration constant is determined by matching the value of $1-u$ at $\mathfrak{R}$ with Eqs. (29) and (30). The value of u at the maximum point is $u_{\max} = 1 - v_{\max}/3$. From Eq. (8), the point that maximizes v must be located on the line P given in Eq. (9), which is not satisfied by $(u_{\max}, v_{\max})$. This indicates that Eq. (34) is an approximate solution with error of $O(1/v_{\max})$, which becomes negligible if the limit $v_{\max} \gg 1$ is taken. Note also that $r_{\max}/r_H = (2/7)^{1/5} \approx 0.7783$ is close to the numerically fitting value in Eq. (27).

Finally, comparing the $r \to 0$ limit of Eq. (34) with Eqs. (16) then using Eqs. (4) and (7), we get the limiting forms for $\nu \ll 1$ as

$$\mu_0 = \frac{2}{15}\left(\frac{16}{15}\right)^2 \nu^{-2}, \qquad \kappa = \left(\frac{16}{15}\right)^2 \nu^{-2}. \tag{35}$$

This implies that both μ_0 and κ diverge quadratically as $\nu \to 0$. Both coefficients are close to their numerical fitting values in Eq. (26). Note that the resulting form for the bare mass

$$m(0) \equiv -\frac{r_H \mu_0}{2} \propto -\frac{r_H}{\nu^2} \tag{36}$$

is formally different from that in Ref. [23] ($\propto -r_H^3$). The difference comes from the fact that the temperature was treated to be that of the black hole in the reference. The density at the center,

$$\rho(r) \to \left(\frac{16}{15}\right)^2 \frac{1}{8\pi\nu^2}\frac{r^2}{r_H^4}, \tag{37}$$

also grows extremely fast.

V. SUMMARY AND DISCUSSIONS

We studied a system of self-gravitating radiation confined in a spherical box by using numerical and analytic calculations. We classified the solution space systematically and defined an AH from the analogy with an apparent horizon. We also analyzed an analytic solution describing a radiation star on the verge of forming a black hole.

Assuming the box to be large enough so that its boundary is located in the asymptotic region, the behavior of the solutions can be summarized as follows: The geometry outside the box is described by the Schwarzschild metric. Around the center, the mass behaves as $m_{\rm r} \propto r^3$ or $m_{\rm s} \propto -m_0 + r^5$ in the absence or in the presence of a central conical singularity, respectively, where r is the areal radial coordinate. On the other hand, for large r, the asymptotic form follows a single formula $m_a \propto 3r/14$. In between the two limits, an AH appears. If the AH is close to an apparent horizon, the transient state $m_t \sim r_{\rm fh}/2 + \epsilon^2 r^3$ arises for a wide range of r just outside of the AH, where ϵ is a very small number.

To classify the solutions, we have designed a set of parameters that characterizes both the internal geometry and the macroscopic quantities. The first parameter ν identifies a solution curve C_ν, a curve on the two-dimensional space of scale-invariant variables $(u,v) \equiv (2m(r)/r, 4\pi r^2 \rho(r))$, which satisfy a first order differential equation originated from the Tollman-Oppenheimer-Volkoff equation. Here, $\nu \equiv 1 - u_H$ represents the orthogonal distance from the solution curve C_ν to the line $u = 1$, where the distance is measured at the AH. In this sense, ν measures how much an AH differs from an apparent horizon. The value of ν is limited to a finite domain $0 \le \nu \le \nu_r \approx 0.50735$. For $\nu = 0$, the AH becomes an apparent horizon. Any solution other than the regular solution with $\nu = \nu_r$ has a conical singularity at the origin. The second parameter r_H represents the size of the AH. It determines the scale of the star described by the solution curve C_ν. Any point on C_ν is parametrized by $(u(\xi), v(\xi))$ where $\xi = \log(r/r_H)$ where $u(\xi)$ and $v(\xi)$ are parametrized functions of ξ. The last parameter is the star size R. Given the three parameters (ν, r_H, R), the ADM mass and the surface temperature are given by $M_R = R u(\xi_R)/2$ and $T = (v(\xi_R)/4\pi\sigma R^2)^{1/4}$, respectively, where $\xi_R = \log(R/r_H)$. Many important physical properties are determined by the sign of ξ_R. For example, if ξ_R is positive ($R > r_H$), the box includes the AH. If ξ_R is negative ($R < r_H$), the system does not include an AH and the contribution of the radiation to the mass is maximized around the surface. For the case of a regular solution, the sign of the heat capacity for a self-gravitating system [3] is also determined by the position of the boundary on the (u, v) plane.

With respect to the behavior near the central singularity, we found mass formulas, $m(0) \propto -r_H/\nu^2$, approximately with respect to the variation of ν. In the $\nu \to 0$ limit, the mass function diverges inverse quadratically, which was shown to be correct by using numerical calculation. The density per unit area also diverges inverse quadratically. The mass and density formula is useful when one studies the behavior of the central conical singularity with respect to the change of macroscopic quantities. In studying the stability of the star, the heat capacity plays a central role. However, the calculation of the heat capacity is nontrivial because of the central singularity of which thermodynamic properties we do not know. If it is possible to ignore the singularity, the heat capacity is determined by the physical values at the boundary similarly to the case of the regular solution in Ref. [3]. In that case, the heat capacity for systems having a boundary just inside of the AH is negative definite. On the other hand, the heat capacity just outside is positive definite even with the geometrical similarity to the event horizon. Far outside of it, a wide approximately constant mass region appears. The geometry in this region resembles that of the Schwarzschild black hole with a

radiation field. Systems having boundary in this region have negative heat capacity once more; whereas, there is a proposal for the thermodynamic properties of the central singularity [22]. Because of this complexity, the stability issues [5,6] should be dealt with cautiously. A way to avoid the complexity due to the central singularity is to place an inner boundary after excising the central part. In this case, the solutions can be used to study a spherical shell of self-gravitating radiations.

ACKNOWLEDGMENTS

This work was supported by Korea National University of Transportation 2016.

[1] D. Lynden-Bell and R. Wood, Mon. Not. R. Astron. Soc. **138**, 495 (1968).
[2] R. D. Sorkin, R. M. Wald, and Z. J. Zhang, Gen. Relativ. Gravit. **13**, 1127 (1981).
[3] D. Pavon and P. T. Landsberg, Gen. Relativ. Gravit. **20**, 457 (1988).
[4] P. H. Chavanis, Astron. Astrophys. **483**, 673 (2008).
[5] P. H. Chavanis, Astron. Astrophys. **381**, 340 (2002).
[6] P. H. Chavanis, C. Rosier, and C. Sire, Phys. Rev. E **66**, 036105 (2002).
[7] H. J. Schmidt and F. Homann, Gen. Relativ. Gravit. **32**, 919 (2000).
[8] M. Schiffer and J. D. Bekenstein, Phys. Rev. D **39**, 1109 (1989).
[9] S. Hod, arXiv:gr-qc/9901035v2.
[10] S. Gao, Springer Proc. Phys. **170**, 359 (2016).
[11] S. Gao, Phys. Rev. D **84**, 104023 (2011); S. Gao, Phys. Rev. D **85**, 027503 (2012).
[12] X. Fang and S. Gao, Phys. Rev. D **90**, 044013 (2014).
[13] J. P. S. Lemos, arXiv:0712.3945.
[14] C. Anastopoulos and N. Savvidou, Classical Quantum Gravity **31**, 055003 (2014).
[15] R. Bousso, Rev. Mod. Phys. **74**, 825 (2002).
[16] R. D. Sorkin, arXiv:gr-qc/9705006v2.
[17] D. N. Page, J. Cosmol. Astropart. Phys. 06 (2014) 051.
[18] D. N. Page and K. C. Phillips, Gen. Relativ. Gravit. **17**, 1029 (1985).
[19] V. Vaganov, arXiv:0707.0864.
[20] S. A. Gentle, M. Rangamani, and B. Withers, J. High Energy Phys. 05 (2012) 106.
[21] A. Pesci, Classical Quantum Gravity **24**, 2283 (2007).
[22] C. Anastopoulos and N. Savvidou, Classical Quantum Gravity **29**, 025004 (2012).
[23] W. H. Zurek and D. N. Page, Phys. Rev. D **29**, 628 (1984).
[24] C. Anastopoulos and N. Savvidou, J. High Energy Phys. 01 (2016) 144.